Electron-impact ionization of Mo^+

J. A. Ludlow, S. D. Loch, and M. S. Pindzola
Department of Physics, Auburn University, Auburn, Alabama 36849, USA
(Received 13 July 2005; published 29 September 2005)

The electron-impact direct ionization cross section for Mo^+ is calculated using both nonperturbative close-coupling and perturbative distorted-wave methods. When distorted-wave calculations for $4d^5 \rightarrow 4d^4$ direct ionization are added to distorted-wave calculations for $4p \rightarrow nl$ excitation-autoionization, the experimental measurements are found to be 60% lower than the theoretical predictions. Inclusion of nonperturbative three-body Coulomb effects, present in time-dependent close-coupling calculations, are found to reduce the distorted-wave $4d^5 \rightarrow 4d^4$ direct ionization cross section by 25%. This is by far the largest reduction yet seen when comparing the two methods for direct subshell ionization of an atomic positive ion in the ground state. However, when the close-coupling calculations for $4d^5 \rightarrow 4d^4$ direct ionization are added to distorted-wave calculations for $4p \rightarrow nl$ excitation-autoionization, the experimental measurements are still 45% lower than the theoretical predictions. Although we further investigate correlation effects in the initial target state and term-dependent potential effects in the ejected electron state in an attempt to understand the small magnitude of the experimental measurements, the discrepancy between theory and experiment remains unexplained.

DOI: 10.1103/PhysRevA.72.032729 PACS number(s): 34.50.Fa

I. INTRODUCTION

An accurate understanding of the electron-impact ionization of atoms and ions is essential for a reliable interpretation of laboratory and astrophysical plasmas. A number of nonperturbative approaches have been developed that successfully account for the three-body Coulomb problem, that of two free electrons moving in the field of an ionized target atom. These include convergent close coupling [1], hyperspherical close coupling [2], *R*-matrix with pseudostates [3], time-dependent close coupling [4], and exterior-complex scaling [5]. For the electron-impact ionization of near-neutral heavy atoms, large discrepancies exist between perturbative theory and experiments. For example, in Mo^+ experimental measurements are found to be 60% lower than perturbative distorted-wave predictions [6], which include both direct and indirect excitation-autoionization contributions. In order to help better understand the possible reasons for this discrepancy, the time-dependent close-coupling method will be used in this paper to calculate the configuration-average $4d^5 \rightarrow 4d^4$ direct ionization cross section for Mo^+.

The time-dependent close-coupling method has been successfully used to calculate electron-impact ionization of many simple atoms and ions. For neutral atoms, perturbative distorted-wave theory tends to overestimate the ground state direct ionization cross section. The close-coupling cross sections are 10% lower than the distorted-wave cross sections at the peak for $H(1s)$ [4], 10% lower at the peak for $He(1s^2)$ [7], 27% lower at the peak for $Li(2s)$ [8,9], 25% lower at the peak for $Be(2s^2)$ [10], and 8% lower at the peak for $C(2p^2)$ [11]. For most singly charged ions, perturbative distorted-wave results are in better agreement with the nonperturbative close-coupling results. The close-coupling cross sections are 10% lower than the distorted-wave cross sections at the peak for $He^+(1s)$ [12], while for $Li^+(1s^2)$ [13] there is good agreement between close-coupling and distorted-wave results. For $Be^+(1s^22s)$ [14], the close-coupling cross sections were found to be 13% lower than the distorted-wave cross sections at the peak, while for $O^+(2p^3)$ [15] there is again good agreement between the close-coupling and distorted-wave results. For more highly charged ions, perturbative distorted-wave theory for ground state direct ionization cross sections is generally quite reliable. We should note, however, that recent studies [16] find that the perturbative distorted-wave method is much less accurate for ionization from excited states than from the ground states of atoms and their ions. We should also note that the configuration-average distorted-wave method becomes quite inaccurate for ground state ionization of near closed shell atoms. The addition of LS term-dependent potentials has been found [17] to reduce the distorted-wave predictions for the direct ionization of Cl and Ar by a factor of 2.

The rest of this paper will proceed as follows. In Sec. II we give a brief outline of the time-independent distorted-wave and time-dependent close-coupling methods that are used to calculate the electron-impact ionization cross section for Mo^+. In Sec. III we present our calculated cross sections and compare with experimental measurements. Finally, in Sec. IV there is a summary of the results. Unless otherwise stated, atomic units are used throughout this paper.

II. THEORY

A. Time-independent distorted-wave method

The configuration-average time-independent distorted-wave (TIDW) expression for the direct ionization cross section of the $(n_t l_t)^{w_t}$ subshell of any atom is given by [18]

$$\sigma = \frac{16 w_t}{k_i^3} \int_0^E \frac{d\left(\frac{k_e^2}{2}\right)}{k_e k_f} \sum_{l_i,l_e,l_f} (2l_i+1)(2l_e+1)(2l_f+1) \times \mathcal{P}(l_i,l_e,l_f,k_i,k_e,k_f), \quad (1)$$

where the linear momenta (k_i,k_e,k_f) and the angular momen-

tum quantum numbers (l_i, l_e, l_f) correspond to the incoming, ejected, and outgoing electron, respectively. The total energy $E=k_i^2/2-I=k_e^2/2+k_f^2/2$, where I is the subshell ionization energy. The first-order scattering probability is given by [18]

$$\mathcal{P}(l_i,l_e,l_f,k_i,k_e,k_f) = \sum_{\lambda} A^{\lambda}_{l_i,l_e,l_f}[R^{\lambda}(k_e l_e, k_f l_f, n_t l_t, k_i l_i)]^2 + \sum_{\lambda'} B^{\lambda'}_{l_i,l_e,l_f}[R^{\lambda'}(k_f l_f, k_e l_e, n_t l_t, k_i l_i)]^2 + \sum_{\lambda}\sum_{\lambda'} C^{\lambda,\lambda'}_{l_i,l_e,l_f} R^{\lambda}(k_e l_e, k_f l_f, n_t l_t, k_i l_i) \times R^{\lambda'}(k_f l_f, k_e l_e, n_t l_t, k_i l_i), \quad (2)$$

where the angular coefficients A, B, C may be expressed in terms of standard 3-j and 6-j symbols and the R^{λ} are standard radial Slater integrals. The incident and scattered continuum electrons were calculated in a V^N potential, while the ejected continuum electron was calculated in a V^{N-1} potential. The continuum normalization for all distorted waves is one times a sine function.

B. Time-dependent close-coupling method

The time-dependent close-coupling (TDCC) equations for an electron scattering from an atom are of the form

$$i\frac{\partial P^{LS}_{l_1 l_2}(r_1,r_2,t)}{\partial t} = T_{l_1 l_2}(r_1,r_2)P^{LS}_{l_1 l_2}(r_1,r_2,t) + \sum_{l_1',l_2'} U^{L}_{l_1 l_2, l_1' l_2'}(r_1,r_2)P^{LS}_{l_1' l_2'}(r_1,r_2,t), \quad (3)$$

where

$$T_{l_1 l_2}(r_1,r_2) = \sum_{i}^{2}\left(-\frac{1}{2}\frac{\partial^2}{\partial r_i^2} + V^{l_i}_{PP}(r_i)\right), \quad (4)$$

$V^{l_i}_{PP}(r)$ is an l-dependent pseudopotential, and

$$U^{L}_{l_1 l_2, l_1' l_2'}(r_1,r_2) = (-1)^{L+l_2+l_2'} \times \sqrt{(2l_1+1)(2l_1'+1)(2l_2+1)(2l_2'+1)} \times \sum_{\lambda} \frac{r^{\lambda}_{<}}{r^{\lambda+1}_{>}} \begin{pmatrix} l_1 & \lambda & l_1' \\ 0 & 0 & 0 \end{pmatrix} \begin{pmatrix} l_2 & \lambda & l_2' \\ 0 & 0 & 0 \end{pmatrix} \times \begin{pmatrix} L & l_2' & l_1' \\ \lambda & l_1 & l_2 \end{pmatrix}. \quad (5)$$

The initial radial wave function is of the form

$$P^{LS}_{l_1 l_2}(r_1,r_2,t=0) = \sqrt{\frac{1}{2}}[\phi_{nl_1}(r_1)g_{kl_2}(r_2) + (-1)^S \phi_{nl_1}(r_2)g_{kl_2}(r_1)], \quad (6)$$

where $g_{kl}(r)$ is a Gaussian radial wave packet with a propagation energy of $k^2/2$. The radial wave function at a time $t=T$ following the collision is obtained by propagating the time-dependent close-coupling equations on a two-dimensional finite lattice. The two electron wave functions fully describe the correlation between the ejected and scattered electrons at all times following the collision. The scattering probability is given by

$$\mathcal{P}(l_i,l_e,l_f,L,S,k_i,k_e,k_f) = \left| \int_0^{\infty} dr_1 \int_0^{\infty} dr_2 \bar{P}_{k_e l_e}(r_1)\bar{P}_{k_f l_f}(r_2)P^{LS}_{l_i l_e l_f}(r_1,r_2,t=T) \right|^2, \quad (7)$$

where $\bar{P}_{kl}(r)$ is a single-particle continuum wave function. The configuration-average time-dependent close-coupling expression for the direct ionization of the $(n_t l_t)^{w_t}$ subshell of any atom is then given by [11]

$$\sigma = \frac{w_t \pi}{4(2l_t+1)k_i^2}\int_0^{E} \frac{d\left(\frac{k_e^2}{2}\right)}{k_e k_f} \sum_{l_i,l_e,l_f}\sum_{L,S}(2L+1)(2S+1) \times \mathcal{P}(l_i,l_e,l_f,L,S,k_i,k_e,k_f), \quad (8)$$

where L is the angular momentum quantum number obtained by coupling l_t and l_i (or l_e and l_f) and S is the spin momentum quantum number obtained by coupling two spin $\frac{1}{2}$ electrons.

C. Generation of the pseudopotential

The $1s^2 2s^2 2p^6 3s^2 3p^6 3d^{10} 4s^2 4p^6 4d^4$ ground state of Mo^{2+} is calculated in the configuration-average Hartree-Fock approximation [19], giving a configuration-average ionization potential for Mo^{2+} of 25.6 eV. These core orbitals are then used to construct the Hamiltonian,

$$h(r) = -\frac{1}{2}\frac{\partial^2}{\partial r^2} + V^{l}_{HX}(r), \quad (9)$$

where

$$V^{l}_{HX}(r) = \frac{l(l+1)}{2r^2} - \frac{Z}{r} + V_H(r) + V_X(r), \quad (10)$$

$V_H(r)$ is the direct Hartree potential, and

$$V_X(r) = -(\alpha_l/2)(24\rho/\pi)^{1/3}$$

is a local exchange potential. For each l, $h(r)$ is diagonalized on a one-dimensional finite lattice. The parameter α_l was varied so that the single particle energies for each angular momentum match the Hartree-Fock configuration-average energy spectrum. For $l=0,1,2$, pseudo-orbitals are then generated by smoothly removing the inner nodes of the wave functions. Using these pseudo-orbitals, the radial Schrodinger equation is then inverted for the l-dependent pseudopotential $V^{l}_{PP}(r)$. For $l>2$, $V^{l}_{PP}(r)=V^{l}_{HX}(r)$. The use of pseudopotentials prevents unphysical excitation of filled subshells during time propagation of the close-coupled equations [14]. The lattice bound state orbitals and their single particle energies are given in Table I.

As a consistency check on the quality of the $\bar{4}d$ pseudo-orbital and how closely it approximates the Hartree-Fock $4d$

TABLE I. Binding energies (in eV) for Mo^+ bound state orbitals on a numerical lattice with 512 points and a mesh spacing of 0.1 a.u.

5*s*	−13.70	5*p*	−9.72	4*d*	−14.56	4*f*	−3.54	5*g*	−2.18
6*s*	−6.12	6*p*	−4.69	5*d*	−5.27	5*f*	−2.26	6*g*	−1.51
7*s*	−3.43	7*p*	−2.79	6*d*	−3.00	6*f*	−1.56	7*g*	−1.10
8*s*	−2.20	8*p*	−1.85	7*d*	−1.96	7*f*	−1.12	8*g*	−0.70
9*s*	−1.52	9*p*	−1.31	8*d*	−1.38	8*f*	−0.70	9*g*	−0.19
10*s*	−1.07	10*p*	−0.87	9*d*	−0.95	9*f*	−0.16		
11*s*	−0.57	11*p*	−0.32	10*d*	−0.44				

orbital, a TIDW ionization cross section was calculated using the $\bar{4}d$ pseudo-orbital. The ionization cross section obtained using the pseudo-orbital was almost identical to that resulting from the use of a Hartree-Fock orbital, giving confidence in the validity of using a pseudo-orbital to represent the Mo^+ ground state.

III. RESULTS

A. Configuration-average calculations

The electron impact ionization of Mo^+ has been investigated previously, both experimentally and theoretically. Crossed-beam experiments have been performed by Man *et al.* [20] and Hathiramani *et al.* [6]. Both experiments have unknown mixtures of ground and metastable states found in both the $4d^5$ and $4d^45s$ configurations. In Fig. 3 of Hathiramani *et al.* [6], the experimental measurements are compared with configuration-average distorted-wave calculations for the $4d^5 \rightarrow 4d^4$ direct ionization cross section. It was found that the experimental measurements are about 40% lower than the direct ionization distorted-wave calculations. A configuration-average distorted-wave calculation for the $4p \rightarrow 4d$ excitation-autoionization contribution yielded an additional 229 Mb at a threshold of 38.2 eV, further increasing the discrepancy with experiment.

New distorted-wave calculations for Mo^+ are compared with the experimental measurements in Figs. 1 and 2. With unknown mixtures of ground and metastable states in the experiments, configuration-average distorted-wave calculations were made for the $4d^5 \rightarrow 4d^4$ direct ionization plus $4p \rightarrow nl$ excitation-autoionization contributions in Fig. 1, and for the $4d^45s \rightarrow 4d^4$ and $4d^45s \rightarrow 4d^35s$ direct ionization plus $4p \rightarrow nl$ excitation-autoionization contributions in Fig. 2. The direct and $4p \rightarrow 4d$ indirect cross sections were statistically partitioned over the energy levels taken from a level-resolved atomic structure calculation [21]. A configuration-average distorted-wave calculation for the higher lying $4p \rightarrow 4f$, $5l$, $6l$, and $7l$ transitions was also carried out, however, they were found to only make a small contribution. The $4d^5$ ground configuration results agree well with the previous calculations [6]. The experimental measurements are found to lie about 60% below theoretical predictions for the $4d^5$ ground configuration, and about 50% below the theoretical predictions for the $4d^45s$ excited configuration, when both direct and indirect ionization processes are taken into account.

The poor performance of perturbative distorted-wave methods in calculating electron impact ionization cross sections for neutral and low-charged heavy atoms is well known. For higher charge states of Mo, distorted-wave calculations perform much better. Distorted-wave calculations including both direct ionization and excitation-autoionization are in good agreement with experiment for Mo^{4+} and Mo^{5+} [6]. It should be noted that semiempirical expressions [22–24] are often used for near-neutrals and generally give good agreement with experiment. However, the semiempirical expressions only account for direct ionization, so the good agreement with experiment is somewhat fortuitous, an overestimate in the direct ionization compensating for the neglect of excitation-autoionization.

Previous theoretical work has demonstrated the inadaquacy of perturbative distorted wave methods and points to the need to attempt a nonperturbative calculation for the electron impact ionization of Mo^+. Thus the nonperturbative TDCC method is used to calculate the direct ionization from the $4d$ subshell of the $4d^5$ ground configuration. The principal advantage of this method is that it accounts for the full Coulomb interaction between the ejected and scattered elec-

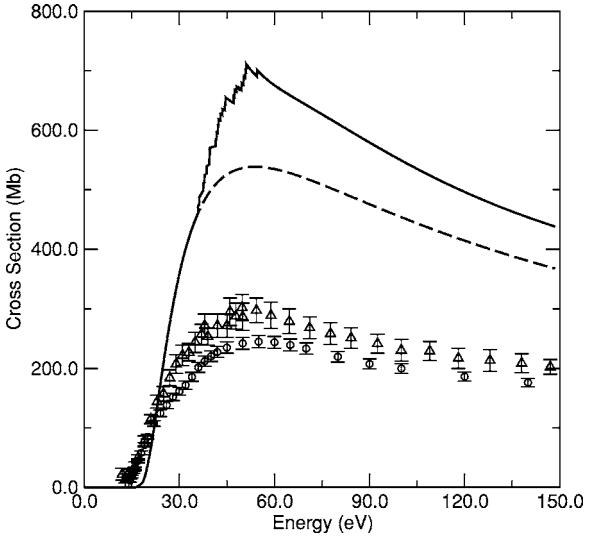

FIG. 1. Electron-impact single ionization cross section for Mo^+ in the $4d^5$ ground configuration. Dashed curve: TIDW calculation for direct ionization, solid curve: TIDW calculation for the sum of direct ionization and $4p \rightarrow nl$ excitation-autoionization, open triangles: experimental measurements [6], and open circles: experimental measurements [20].

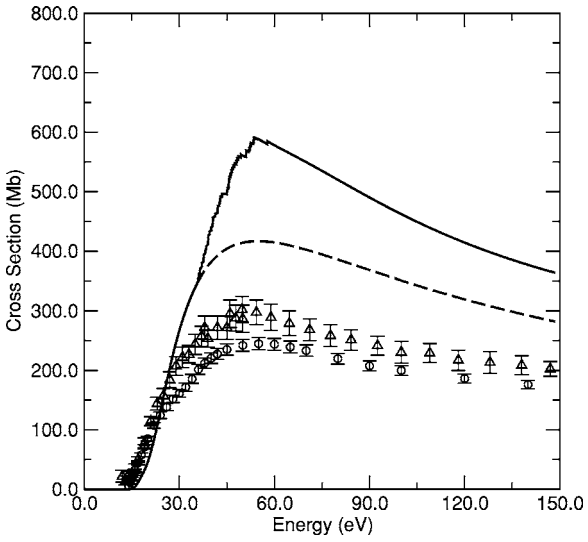

FIG. 2. Electron-impact single ionization cross section for Mo^+ in the $4d^45s$ excited configuration. Dashed curve: TIDW calculation for direct ionization, solid curve: TIDW calculation for the sum of direct ionization and $4p \rightarrow nl$ excitation-autoionization, open triangles: experimental measurements [6], and open circles: experimental measurements [20].

trons as they receed in the long-range Coulomb field of the Mo^{2+} core.

Partial-wave direct ionization cross sections for Mo^+ calculated using the time-dependent close-coupling method are presented in Table II. The TDCC equations are solved on a numerical lattice with 512 points in each radial direction with a mesh spacing of 0.1 a.u., giving a box size of 51.2 a.u. The propagation time needed to converge the collision probabilities varies with the collision energy, the higher the collision energy, the shorter the time needed. The number of $(l_1 l_2)$ coupled channels used in the calculations varied from 7 for $L=0$ to 24 for $L=8$. Ionization cross sections at 40, 50, 70, and 100 eV are calculated. The presence of an outer d subshell in Mo^+ complicates matters. In this case, for a particular total angular momentum L of the bound and incident electrons, the incoming electron has its own individual angular momentum l. Therefore, for a particular total L, the TDCC equations must be solved separately for different asympotic boundary conditions on the incoming electron's angular momentum. For example, for an s-wave incident electron, we need to solve the TDCC equations for ^1D and ^3D symmetries. For a p-wave incident electron, $^1P, ^3P, ^1D, ^3D, ^1F, ^3F$ symmetries have to be calculated and for a d-wave incident electron, $^1S, ^3S, ^1P, ^3P, ^1D, ^3D, ^1F, ^3F, ^1G, ^3G$ symmetries are needed. So for p-wave scattering, the calculation is three times as difficult as for the ionization of an ns subshell, while for d-wave scattering and above, the calculation is five times as difficult. TDCC results were calculated for incoming electron angular momenta from $l=0$ to $l=6$. By $l=6$, TIDW calculations for the direct ionization are in good agreement with the TDCC calculations. Therefore, for $l=7 \rightarrow 50$ TIDW results were used to "top-up" the TDCC results. In Fig. 3 the TDCC results are compared with TIDW results for direct ionization. At the peak of the cross section, the TDCC results are about 25% lower than the distorted wave. This difference between the TDCC and TIDW results is the biggest seen thus far for TDCC calculations on singly charged positive ions and demonstrates the importance of properly accounting for long-range Coulomb interactions. Note that the solid curve is a smooth fit, starting at the ionization energy, through the four closed square data points.

The same configuration-average TDCC calculations for direct ionization from the $4d$ subshell of the $4p^64d^5$ ground configuration also yield direct excitation cross sections for the $4p^64d^5 \rightarrow 4p^64d^4nl$ transitions. In fact, the ionization collision probability may also be calculated by summing all nl excitation collision probabilities and subtracting from one. However, new configuration-average TDCC calculations for direct ionization from the $4p$ subshell of the $4p^64d^5$ ground configuration are needed to obtain excitation-autoionization cross sections for the $4p^64d^5 \rightarrow 4p^54d^6$ and $4p^64d^5 \rightarrow 4p^54d^5nl$ transitions.

TABLE II. Partial ionization cross sections (Mb) for Mo^+ at four incident electron energies. l_i is the incident angular momentum.

	40 eV		50 eV		70 eV		100 eV	
l_i	TDCC	TIDW	TDCC	TIDW	TDCC	TIDW	TDCC	TIDW
0	6.47	7.08	5.36	6.13	3.63	4.75	2.23	3.49
1	42.6	38.3	40.9	30.4	33.2	19.8	22.7	12.8
2	24.5	101.4	21.2	84.2	14.7	56.4	5.9	32.0
3	72.7	140.3	81.0	143.7	69.2	115.6	42.4	72.6
4	91.9	96.6	81.7	101.6	56.3	82.4	32.1	50.6
5	49.1	50.6	54.1	59.4	52.4	60.9	42.3	51.2
6	31.6	30.7	38.0	39.6	41.4	45.8	37.2	43.0
0–6	323.9	464.9	326.1	465.0	270.8	385.7	184.9	265.6
7–50		48.7		80.9		132.0		180.1
Total Cross section	372.5	513.6	406.9	545.9	402.8	517.7	364.9	445.7

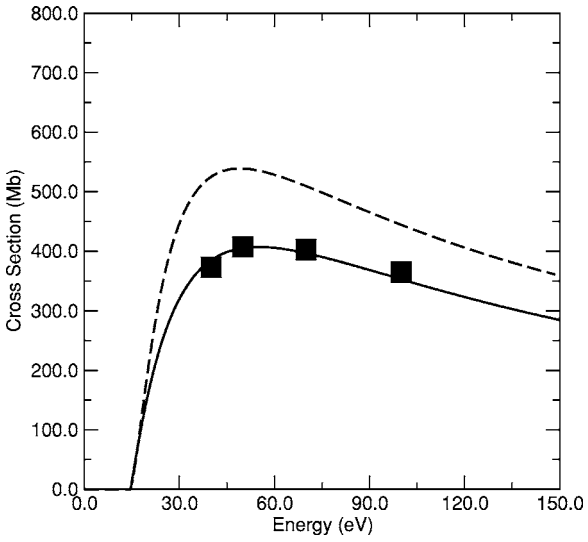

FIG. 3. Direct ionization cross section for Mo^+ in the $4d^5$ ground configuration. Dashed curve: TIDW calculation, closed squares connected by solid curve: TDCC calculation.

The nonperturbative close-coupling calculations for the $4d^5 \rightarrow 4d^4$ direct ionization plus the perturbative distorted-wave calculations for the $4p \rightarrow nl$ excitation-autoionization contributions are compared with the Mo^+ experiments in Fig. 4. The experimental measurements are found to now lie about 45% below the theoretical predictions at the peak of the cross section. We could scale our perturbative distorted-wave calculations for direct ionization from the $4d^45s$ excited configuration to match the nonperturbative close-coupling reduction of 25% found for direct ionization from the $4d^5$ ground configuration. Thus, assuming that only the levels of the $4d^45s$ excited configuration are populated, the experimental measurements would still lie about 35% below the theoretical predictions at the peak of the cross section.

B. Beyond configuration-average calculations

There are a couple of factors that may account for the remaining discrepancy between theory and experiment. Correlation in the initial state may affect the total ionization cross section. However, it was realized a number of years ago that contributions from excited configurations that mix with the ground configuration add incoherently for total ionization cross sections [25]. Thus an estimate of the strength of configuration-interaction effects is given by the square of the mixing coefficients. As an example, for He the $1s^2$ ground configuration will mix with the $2s^2$ and $2p^2$ excited configurations, with multiconfiguration mixing coefficients $c_{1s}=0.9962$, $c_{2s}=-0.0619$, and $c_{2p}=0.0620$ [26]. So for He, ground state correlation should not have a strong effect on the ionization cross section. This was confirmed recently by nonperturbative TDCC calculations of electron impact single and double ionization of He($1s^2$) [27]. Three-dimensional calculations were made using an exact ground state obtained by relaxing the Schrodinger equation in imaginary time. Therefore ground state correlation of the form He($1s^2+2s^2+2p^2+\cdots$) is automatically included. The 3D TDCC calculations were compared with 2D TDCC calculations made using a frozen core approximation for ionization from the $1s^2$ configuration. The two calculations were found to be in excellent agreement, confirming the mixing coefficient argument.

Even in the case of the electron-impact ionization of Be, with mixing coefficients of $c_{2s} \approx 0.95$ and $c_{2p} \approx 0.31$ [28] for the $2s^2+2p^2$ multiconfiguration ground state, it was found that the inclusion of ground state correlation in a perturbative distorted wave calculation only produced a small 5%–10% change in the ionization cross section [25]. The influence of initial state correlation in Mo^+ was investigated by performing ($4d^5+4d^34f^2$) multiconfiguration Hartree-Fock calculations [26]. For the lowest two LS terms of the 16 allowed, the mixing coefficient for the $4d^5$ configuration is found to be 0.9929 for ^6S and 0.9935 for ^4G. Thus the inclusion of initial state correlation does not seem sufficient to explain the discrepancy with experiment for the electron ionization of Mo^+.

Term-dependent effects in the core potentials may affect the total ionization cross section. The close-coupling results presented in this paper used approximate configuration-average potentials for the time evolution of the wave packet, while the distorted-wave results used approximate configuration-average potentials for the incident, ejected, and scattered electron wave functions. Previous LS term resolved distorted-wave calculations [17] for the $3p^6\ ^1S \rightarrow 3p^5\ ^2P$ ionization of Ar and the $3p^5\ ^2P \rightarrow 3p^4\ (^3P, ^1D, ^1S)$ ionization of Cl have shown dramatic changes in the cross sections when term-dependent potentials are used for the ejected electron. To test the possible effect of term-dependent potentials in electron ionization of Mo^+, we carried out LS term resolved distorted-wave calculations for the $4d^5\ ^6S \rightarrow 4d^4\ ^5D$ transition, one of the 256 possible LS transitions involving the $4d^5 \rightarrow 4d^4$ configuration transition. Upon examination of the 38 possible continuum Hartree-Fock equations for the $l=0-3$ ejected electrons, we found that the term-dependent potential for the $4d^4\ ^5Dkd\ ^6S$ term is given by

$$V = V_{core} + 4J^0_{4d} - \frac{2}{7}J^2_{4d} - \frac{2}{7}J^4_{4d} + 4K^0_{4d} - \frac{2}{7}K^2_{4d} - \frac{2}{7}K^4_{4d}, \tag{11}$$

while the configuration-average potential for the $4d^4kd$ configuration is given by

$$V = V_{core} + 4J^0_{4d} - \frac{2}{5}K^0_{4d} - \frac{4}{35}K^2_{4d} - \frac{4}{35}K^4_{4d}, \tag{12}$$

where J^λ_{nl} and K^λ_{nl} are direct and exchange potential operators [17].

Our distorted-wave calculations for the $4d^5\ ^6S \rightarrow 4d^4\ ^5D$ direct ionization of Mo^+ are presented in Fig. 5. The dashed curve in Fig. 5 is a distorted-wave calculation using approximate configuration-average potentials. Apart from a scaled energy shift due to the difference in ionization potentials of the $4d^5\ ^6S \rightarrow 4d^4\ ^5D$ term transition and the $4d^5 \rightarrow 4d^4$ configuration transition, the LS resolved cross section of Fig. 5 using configuration-average potentials agrees with the configuration-average cross section of Fig. 1, since the ion-

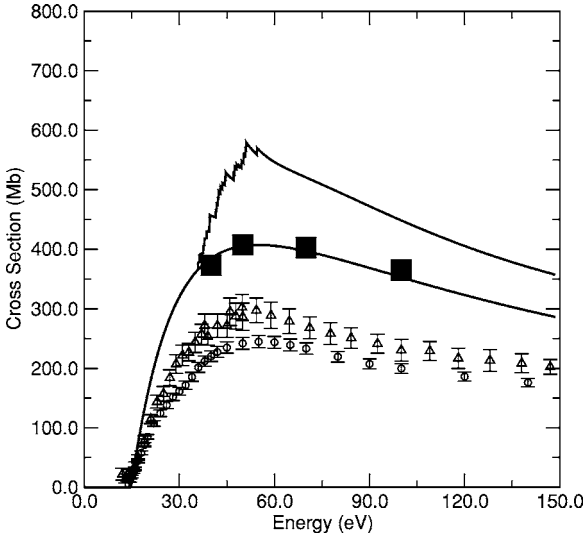

FIG. 4. Electron-impact single ionization cross section for Mo^+ in the $4d^5$ ground configuration. Closed squares connected by solid curve: TDCC calculation for direct ionization, solid curve: TDCC calculation for direct ionization plus TIDW calculation for $4p \rightarrow nl$ excitation-autoionization, open triangles: experimental measurements [6], and open circles: experimental measurements [20].

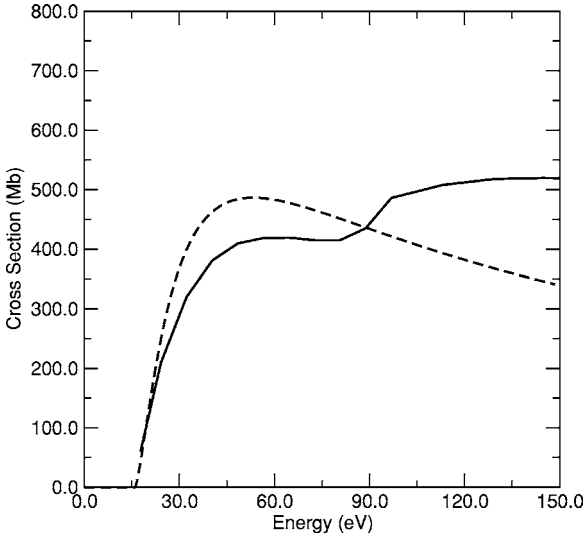

FIG. 5. Direct ionization cross section for the $4d^5\,{}^6S \rightarrow 4d^4\,{}^5D$ transition in Mo^+, dashed curve: configuration-average TIDW calculation, solid curve: term-dependent TIDW calculation.

ization branching fraction [29], $B=[c(d^4\,{}^5D|\}d^5\,{}^6S)]^2=1$, where c is a coefficient of fractional parentage. The solid curve in Fig. 5 is a distorted-wave calculation in which the full Hartree-Fock potential of Eq. (11) is used for the $4d^4\,{}^5Dkd\,{}^6S$ ejected electron wave functions. The LS resolved cross section of Fig. 5 using term-dependent potentials shows a pronounced steplike feature around 90 eV incident electron energy. This is due to a shape resonance caused by the large positive monopole exchange term of Eq. (11).

Although this particular term-dependent potential effect is quite dramatic for the $4d^5\,{}^6S \rightarrow 4d^4\,{}^5D$ transition, it would be somewhat washed out in transitions from the four quartet $4d^5$ initial terms to the one quintet and seven triplet $4d^4$ final terms, and would not be present at all in the transitions from the 11 doublet $4d^5$ initial terms, when calculated in the perturbative distorted-wave approximation. Furthermore, term-dependent effects in other triplet and singlet $4d^4$ final terms are probably not as strong as that found in the quintet term of Fig. 5. Thus the inclusion of term-dependent potential effects does not seem sufficient to explain the discrepancy with experiment for the electron ionization of Mo^+.

An ideal choice for the inclusion of initial target correlation, term-dependent potential effects for the ejected electron, and the three-body interactions between the scattered and ejected electrons moving in Coulomb field of the atomic core is the R-matrix with pseudo-states method [30,31]. However, to check our distorted-wave results for the $4d^5\,{}^6S \rightarrow 4d^4\,{}^5D$ transition between LS terms using a minimum of $l=0-4$ and $n=4-12$ pseudostates would require 315 coupled LS terms. To check our close-coupling and distorted-wave results for the $4d^5 \rightarrow 4d^4$ transition between configurations would require at least an order of magnitude increase in the number of coupled terms. Finally, one would also like to include additional coupled terms associated with the $4d^4 5s$ initial excited configuration, as well as possible terms to handle $4d^2 \rightarrow 4f^2$ initial state correlation. Certainly, a calculation awaiting the next generation of computers.

IV. SUMMARY

In this paper, we calculated the electron-impact single ionization cross section of Mo^+ using nonperturbative close-coupling and perturbative distorted-wave methods. It is found that the close-coupling results are 25% lower than the distorted-wave results for the $4d^5 \rightarrow 4d^4$ direct ionization cross section. This is the largest difference that has been found between perturbative and nonperturbative calculations for electron impact ionization of singly charged positive ions in their ground state. However, the experimental measurements are found to be about 45% below our theoretical predictions at the peak of the cross section, when both direct and indirect ionization processes are included. To better understand the discrepancy between theory and experiment, we also investigated correlation effects in the initial target state and term-dependent potential effects in the ejected electron state. Neither of these two effects seems to be sufficient to explain the discrepancy. Further progress on the theory side might involve a truly large scale computational effort, while progress on the experimental side might involve a better understanding of the ground and metastable state populations and measurements of individual LS term resolved ionization cross sections.

ACKNOWLEDGMENTS

This work was supported in part by the U.S. Department of Energy's Office of Fusion Energy Sciences. Computational work was carried out at the National Energy Research Scientific Computing Center in Oakland, CA.

[1] I. Bray and A. T. Stelbovics, Phys. Rev. Lett. **70**, 746 (1993).
[2] D. Kato and S. Watanabe, Phys. Rev. Lett. **74**, 2443 (1995).
[3] K. Bartschat and I. Bray, J. Phys. B **29**, L577 (1996).
[4] M. S. Pindzola and F. Robicheaux, Phys. Rev. A **54**, 2142 (1996).
[5] C. W. McCurdy, M. Baertschy, and T. N. Rescigno, J. Phys. B **37**, R137 (2004).
[6] D. Hathiramani, K. Aichele, G. Hofmann, M. Steidl, M. Stenke, R. Volpel, E. Salzborn, M. S. Pindzola, J. A. Shaw, D. C. Griffin, and N. R. Badnell, Phys. Rev. A **54**, 587 (1996).
[7] M. S. Pindzola and F. J. Robicheaux, Phys. Rev. A **61**, 052707 (2000).
[8] J. Colgan, M. S. Pindzola, D. M. Mitnik, and D. C. Griffin, Phys. Rev. A **63**, 062709 (2001).
[9] J. Colgan, M. S. Pindzola, D. M. Mitnik, D. C. Griffin, and I. Bray, Phys. Rev. Lett. **87**, 213201 (2001).
[10] J. Colgan, S. D. Loch, M. S. Pindzola, C. P. Ballance, and D. C. Griffin, Phys. Rev. A **68**, 032712 (2003).
[11] M. S. Pindzola, J. Colgan, F. Robicheaux, and D. C. Griffin, Phys. Rev. A **62**, 042705 (2000).
[12] M. C. Witthoeft, M. S. Pindzola, and J. Colgan, Phys. Rev. A **67**, 032713 (2003).
[13] M. S. Pindzola, D. M. Mitnik, J. Colgan, and D. C. Griffin, Phys. Rev. A **61**, 052712 (2000).
[14] M. S. Pindzola, F. Robicheaux, N. R. Badnell, and T. W. Gorczyca, Phys. Rev. A **56**, 1994 (1997).
[15] S. D. Loch, J. Colgan, M. S. Pindzola, M. Westermann, F. Scheuermann, K. Aichele, D. Hathiramani, and E. Salzborn, Phys. Rev. A **67**, 042714 (2003).
[16] D. C. Griffin, C. P. Ballance, M. S. Pindzola, F. Robicheaux, S. D. Loch, J. A. Ludlow, M. C. Witthoeft, J. Colgan, C. J. Fontes, and D. R. Schultz, J. Phys. B **38**, L199 (2005).
[17] D. C. Griffin, M. S. Pindzola, T. W. Gorczyca, and N. R. Badnell, Phys. Rev. A **51**, 2265 (1995).
[18] M. S. Pindzola, D. C. Griffin, and C. Bottcher, in *Atomic Processes in Electron-ion and Ion-ion Collisions*, Vol. 145 of *NATO Advanced Study Institute, Series B: Physics*, edited by F. Brouillard (Plenum, New York, 1986), p. 75.
[19] C. F. Fischer, Comput. Phys. Commun. **43**, 355 (1987).
[20] K. F. Man, A. C. H. Smith, and M. F. A. Harrison, J. Phys. B **20**, 1351 (1987).
[21] R. D. Cowan, *The Theory of Atomic Structure and Spectra* (University of California Press, Berkeley, 1981).
[22] W. Lotz, Z. Phys. **216**, 241 (1968).
[23] Y. K. Kim and M. E. Rudd, Phys. Rev. A **50**, 3954 (1994).
[24] Y. K. Kim and P. M. Stone, Phys. Rev. A **64**, 052707 (2001).
[25] S. M. Younger, Phys. Rev. A **24**, 1278 (1981).
[26] C. F. Fischer, T. Brage, and P. Jonsson, *Computational Atomic Structure: An MCHF Approach* (IOP, Bristol, 1997).
[27] M. S. Pindzola, F. J. Robicheaux, J. P. Colgan, M. C. Witthoeft, and J. A. Ludlow, Phys. Rev. A **70**, 032705 (2004).
[28] J. C. Morrison and C. F. Fischer, Phys. Rev. A **35**, 2429 (1987).
[29] D. H. Sampson, Phys. Rev. A **34**, 986 (1986).
[30] K. Bartschat, Comput. Phys. Commun. **114**, 168 (1998).
[31] C. P. Ballance, D. C. Griffin, J. A. Ludlow, and M. S. Pindzola, J. Phys. B **37**, 4779 (2004).